Toxicology 283 (2011) 101–108

Contents lists available at ScienceDirect

Toxicology

journal homepage: www.elsevier.com/locate/toxicol

Oxidative stress mediated apoptosis induced by nickel ferrite nanoparticles in cultured A549 cells

Maqusood Ahamed[a,*], Mohd Javed Akhtar[b], Maqsood A. Siddiqui[c], Javed Ahmad[c], Javed Musarrat[c], Abdulaziz A. Al-Khedhairy[c], Mohamad S. AlSalhi[a], Salman A. Alrokayan[a]

[a] King Abdullah Institute for Nanotechnology, King Saud University, Riyadh 11451, Saudi Arabia
[b] Fibre Toxicology Division, Indian Institute of Toxicology Research, Lucknow 226001, India
[c] Al-Jeraisy Chair for DNA Research, Department of Zoology, King Saud University, Riyadh 11451, Saudi Arabia

ARTICLE INFO

Article history:
Received 10 January 2011
Received in revised form 24 February 2011
Accepted 28 February 2011
Available online 4 March 2011

Keywords:
Nickel ferrite nanoparticles
Oxidative stress
Apoptosis
p53
Survivin

ABSTRACT

Due to the interesting magnetic and electrical properties with good chemical and thermal stabilities, nickel ferrite nanoparticles are being utilized in many applications including magnetic resonance imaging, drug delivery and hyperthermia. Recent studies have shown that nickel ferrite nanoparticles produce cytotoxicity in mammalian cells. However, there is very limited information concerning the toxicity of nickel ferrite nanoparticles at the cellular and molecular level. The aim of this study was to investigate the cytotoxicity, oxidative stress and apoptosis induction by well-characterized nickel ferrite nanoparticles (size 26 nm) in human lung epithelial (A549) cells. Nickel ferrite nanoparticles induced dose-dependent cytotoxicity in A549 cells demonstrated by MTT, NRU and LDH assays. Nickel ferrite nanoparticles were also found to induce oxidative stress evidenced by generation of reactive oxygen species (ROS) and depletion of antioxidant glutathione (GSH). Further, co-treatment with the antioxidant L-ascorbic acid mitigated the ROS generation and GSH depletion due to nickel ferrite nanoparticles suggesting the potential mechanism of oxidative stress. Quantitative real-time PCR analysis demonstrated that following the exposure of A549 cells to nickel ferrite nanoparticles, the level of mRNA expressions of cell cycle checkpoint protein p53 and apoptotic proteins (bax, caspase-3 and caspase-9) were significantly up-regulated, whereas the expression of anti-apoptotic proteins (survivin and bcl-2) were down-regulated. Moreover, activities of caspase-3 and caspase-9 enzymes were also significantly higher in nickel ferrite nanoparticles exposed cells. To the best of our knowledge this is the first report showing that nickel ferrite nanoparticles induced apoptosis in A549 cells through ROS generation and oxidative stress via p53, survivin, bax/bcl-2 and caspase pathways.

1. Introduction

Spinel ferrite nanoparticles with the general formula MFe_2O_4 (where M is +2 cation of Ni, Mn, Zn or Co) are very important materials because of their interesting magnetic and electrical properties with good chemical and thermal stabilities (Willard et al., 2004). These nanocrystalline materials are used in many applications including magnetic extraction, magnetic resonance imaging, cell labeling, drug delivery and hyperthermia (Lee et al., 2007; Rana et al., 2007; Sun et al., 2008; Chertok et al., 2008). Hyperthermia is a method of cancer treatments which is designed to raise the temperature of cancer cells. Cancer cells more are susceptible to heat than normal cells. Hyperthermia treatment thus has the advantage of being less risky to the body, with fewer side effects (Tomitaka et al., 2010). Nickel ferrite ($NiFe_2O_4$) is one of the most important spinel ferrites. Despite the wide-spread application of nickel ferrite nanoparticles, there is a serious lack of information concerning the toxicity of these nanoparticles at the cellular and molecular level. Only a few significant studies reported potential cytotoxicity of spinet ferrite nanoparticles including nickel ferrite nanoparticles (Yin et al., 2005; Baldi et al., 2007; Beji et al., 2010). Tomitaka et al. (2009) reported that nickel ferrite nanoparticles showed only minimal changes on HeLa cell proliferation at concentrations of 10 μg/ml, but significantly low viability at concentrations of 100 μg/ml (Tomitaka et al., 2009).

The molecular mechanisms of toxicity of nanoparticles are still underway. One mechanism frequently discussed is the induction of oxidative damage of cellular constituents, either due to the generation of reactive oxygen species (ROS) or by inactivation of antioxidant defense system (Nel et al., 2006; Stone and Donaldson, 2006). Experimental evidence has shown that metal and metal oxide nanoparticles induced DNA damage and apoptosis through

* Corresponding author. Tel.: +966 4670662; fax: +966 4670664.
E-mail address: maqusood@gmail.com (M. Ahamed).

0300-483X/$ – see front matter © 2011 Elsevier Ireland Ltd. All rights reserved.
doi:10.1016/j.tox.2011.02.010

ROS generation and oxidative stress (Park et al., 2008; Asharani et al., 2009; Ahamed et al., 2010a,b; Lunov et al., 2010). For example, our previous studies have shown that silver nanoparticles, copper oxide nanoparticles and silica nanoparticles induced cytotoxicity, DNA damage and apoptosis in cultured human cells through lipid peroxidation, ROS generation and oxidative stress (Ahamed et al., 2008, 2010c; Akhtar et al., 2010a).

Apoptosis is controlled by a large number of genes acting as death switches. The tumor suppressor gene p53 is regarded as the guardian of the cell genome is able to activate cell cycle checkpoints, DNA repair and apoptosis to maintain stability of genome (Sherr, 2004). In the presence of cellular stress, p53 triggers cell cycle arrest to provide time for the damage to be repaired or self-mediated apoptosis (Farnebo et al., 2010). Survivin, one member of inhibitor of apoptosis family, has recently been reported to play an important role in both cell proliferation and cell death. Down-regulation of survivin expression may cause a cell-cycle defect that leads to apoptotic cell death (Ryan et al., 2009). The bcl-2 and bax are two discrete members of a gene family also involved in the regulation of apoptosis. The bcl-2 blocks cell death following various stimuli, demonstrating a death-sparing effect; however, over expression of bax has a pro-apoptotic effect and bax also counters the anti-apoptotic activity of bcl-2 (Chougule et al., 2010). The ratio of bax to bcl-2 expression represents a cell death switch, which determines the life or death of cells in response to an apoptotic stimulus; an increased bax/bcl-2 ratio decreases the cellular resistance to apoptotic stimuli, leading to increased apoptotic cell death (Bai and Meng, 2005; Gao and Wang, 2009). It has also been well documented that signaling pathway leading to apoptosis involved the sequential activation of cysteine proteases known as caspases (Takadera and Ohyashiki, 2007; Tang et al., 2010). The present study was designed to investigate the nickel ferrite nanoparticles induced apoptosis through ROS generation and oxidative stress via p53, survivin, bax/bcl-2 and caspase pathways in human lung epithelial A549 cells. This preliminary study provides insight into nickel ferrite nanoparticles induced apoptotic cell death in A549 cells and possible cellular and molecular mechanisms involved. Human lung epithelial A549 cells, derived from human lung carcinoma, have widely been used to study the cytotoxicity, ROS generation, oxidative stress and molecular mechanisms of apoptosis (Sánchez-Pérez et al., 2009; Ye et al., 2009; Ahamed et al., 2010c; Akhtar et al., 2010a,b; Barillet et al., 2010; Zhang et al., 2010).

2. Materials and methods

2.1. Nickel ferrite nanoparticles and reagents

Nickel ferrite ($NiFe_2O_4$) nanopowder (Product No. 637149, particle size: <50 nm and purity: ≥98% trace metals basis), MTT ([3-(4,5-dimethylthiazol-2-yl)-2,5-diphenyltetrazoliumbromide]), reduced glutathione (GSH), DTNB (5,5-dithio-bis-(2-nitrobenzoic acid)), DCFH-DA (2,7-dichlorofluorescin diacetate) and L-ascorbic acid (AA) were purchased from Sigma–Aldrich, USA. Fetal bovine serum (FBS), penicillin–streptomycin, DMEM/F-12 medium and HBSS were obtained from Invitrogen Co., USA. All other chemicals used were of the highest purity available from commercial sources.

2.2. Characterization of nickel ferrite nanoparticles

The crystalline nature of nickel ferrite nanopowder was carried out by taking X-ray diffraction (XRD) pattern at room temperature with the help of PANalytical X'Pert X-ray diffractometer equipped with a Ni filtered using Cu K_α ($\lambda = 1.54056$ Å) radiations as X-ray source. Morphology and size of the nanoparticles was examined by field emission scanning electron microscope (FESEM, JSM-7600F, JEOL Inc.) and field emission transmission electron microscopy (FETEM, JEM-2100F, JEOL Inc.) at an accelerating voltage of 15 kV and 200 kV respectively. Briefly, suspension of nickel ferrite nanoparticles was sonicated using a sonicator bath at room temperature for 15 min at 40 W to form a homogeneous suspension. Further, a drop of aqueous nanoparticles was placed onto a carbon-coated copper TEM grid, air-dried and observed with TEM. Energy dispersive X-ray (EDX) analysis was used to see the elemental composition of the nanocrystalline nickel ferrite.

Dynamic light scattering (DLS) (ZetaSizer-HT) was used to determine the hydrodynamic size the nickel ferrite nanoparticles suspension in the cell culture medium. Nanoparticles were suspended in cell culture media, sonicated at room temperature for 10 min at 40 W to form homogeneous mixture and DLS was performed.

2.3. Cell culture and treatment of nickel ferrite nanoparticles

Human lung epithelial A549 cells were used between passages 10 and 20. Cells were cultured in DMEM/F-12 medium supplemented with 10% FBS and 100 U/ml penicillin–streptomycin at 5% CO_2 and 37 °C. At 85% confluence, cells were harvested using 0.25% trypsin and were sub-cultured into 75 cm^2 flasks, 6-well plates or 96-well plates according to selection of experiments. Cells were allowed to attach the surface for 24 h prior to treatment. Nickel ferrite nanoparticles were suspended in cell culture medium and diluted to appropriate concentrations. The dilutions of nickel ferrite nanoparticles were then sonicated using a sonicator bath at room temperature for 10 min at 40 W to avoid nanoparticles agglomeration prior to administration to the cells.

2.4. MTT assay

Viability of A549 cells after exposure to nickel ferrite nanoparticles was assessed by MTT assay as described by Mossman (1983). The MTT assay assesses the mitochondrial function by measuring ability of viable cells to reduce MTT into blue formazon product. In brief, 1×10^4 cells/well were seeded in 96-well plates and exposed to nanoparticles at the concentrations of 0, 1, 2, 5, 10, 25, 50 and 100 μg/ml for 24 h. After the exposure completed, the medium was removed from each well to avoid interference of nanoparticles and replaced with new medium containing MTT solution in an amount equal to 10% of culture volume, and incubated for 3 h at 37 °C until a purple colored formazan product developed. The resulting formazan product was dissolved in acidified isopropanol. Further, the 96-well plate was centrifuged at 2500 rpm for 5 min to settle down the remaining nanoparticles present in the solution. Then, a 100 μl supernatant was transferred to other fresh wells of 96-well plate and absorbance was measured at 570 by using a microplate reader (Synergy-HT, BioTek).

2.5. NRU assay

Neutral red uptake (NRU) assay was performed following the procedure as described by Borenfreund and Puerner (1984) with some modifications (Siddiqui et al., 2010). In brief, 1×10^4 cells/well were seeded in 96-well plates and exposed to nickel ferrite nanoparticles at the concentrations of 0, 1, 2, 5, 10, 25, 50 and 100 μg/ml for 24 h. At the end of exposure the test solution was aspirated and cells were washed with PBS twice and incubated for 3 h in medium supplemented with neutral red (50 μg/ml). The medium was washed off rapidly with a solution containing 0.5% formaldehyde and 1% calcium chloride. Cells were further incubated for 20 min at 37 °C in a mixture of acetic acid (1%) and ethanol (50%) to extract the dye. The plates were finally read at 540 nm using microplate reader (Synergy-HT, BioTek).

2.6. LDH leakage assay

Lactate dehydrogenase (LDH) is an enzyme widely present in cytosol that converts lactate to pyruvate. When plasma membrane integrity is disrupted, LDH leaks into culture media and its extracellular level is elevated (Wroblewski and LaDue, 1955). LDH assay was carried out by the LDH-Cytotoxicity assay kit (Bio-Vision) according to the manufacturer's protocol. In brief, 1×10^4 cells/well were seeded in 96-well plates and exposed to nickel ferrite nanoparticles at the concentrations of 0, 1, 2, 5, 10, 25, 50 and 100 μg/ml for 24 h. After the exposure completed, the 96-well plate was centrifuged at 2500 rpm for 5 min to settle down the nanoparticles present in the solution. A 100 μl of supernatant transferred to new fresh well of 96-well plate that already containing 100 μl reaction mixture from BioVision kit and incubated for 30 min at room temperature. After incubation, the absorbance of solution was measured at 340 by using a microplate reader (Synergy-HT, BioTek). LDH levels in the media versus the cells were quantified and compared to the control values according to the instruction of kit.

2.7. Measurement of ROS and GSH

Oxidative stress markers (ROS and GSH) were determined in A549 cells exposed to 100 μg/ml nickel ferrite nanoparticles for 24 h. Antioxidant ascorbic acid (1.5 mM) was co-exposed with or without nickel ferrite nanoparticles to delineate the potential mechanism of oxidative stress.

The production of intracellular ROS was measured using 2,7-dichlorofluorescin diacetate (DCFH-DA) (Wang and Joseph, 1999). The DCFH-DA passively enters the cell where it reacts with ROS to form the highly fluorescent compound dichlorofluorescein (DCF). Briefly, 10 mM DCFH-DA stock solution (in methanol) was diluted in culture medium without serum or other additive to yield a 100 μM working solution. At the end of exposure with nanoparticles and L-ascorbic acids cells were washed twice with HBSS. Then cells were incubated in 1 ml working solution of DCFH-DA at 37 °C for 30 min. Cells were lysed in alkaline solution and centrifuged at 2300 × *g*. A

200 μl supernatant was transferred to 96-well plate and fluorescence was measured using at 485 nm excitation and 520 nm emission using a microplate reader (Synergy-HT, BioTek). The values were expressed as percent of fluorescence intensity relative to control wells.

For the measurement of GSH, cells were cultured in 75-cm^2 culture flask. After the treatment cell pellets from control and treated group were then lysed in cell lysis buffer [1 × 20 mM Tris–HCl (pH 7.5), 150 mM NaCl, 1 mM Na_2EDTA, 1% Triton, 2.5 mM sodium pyrophosphate]. Following centrifugation (15,000 × *g* for 10 min at 4 °C) the supernatant (cell extract) was maintained on ice until assayed for the cellular GSH using Ellman's method (1959). Briefly, a mixture of 0.1 ml of cell extract and 0.9 ml of 5% TCA was centrifuged (2300 × *g* for 15 min at 4 °C). Then 0.5 ml of supernatant added into 1.5 ml of 0.01% DTNB and the reaction was monitored at 412 nm. The amount of GSH was expressed in terms of nmol/mg protein.

2.8. Total RNA isolation and quantitative real-time PCR analysis of apoptotic markers

For total RNA isolation, A549 cells were cultured in 6-well plates and exposed to nickel ferrite nanoparticles at a concentration of 100 μg/ml for 24 h. At the end of exposure total RNA was extracted by RNeasy mini Kit (Qiagen) according to the manufacturer's instructions. Concentration of the extracted RNA was determined using Nanodrop 8000 spectrophotometer (Thermo-Scientific) and the integrity of RNA was visualized on 1% agarose gel using gel documentation system (Universal Hood II, BioRad). The first strand cDNA was synthesized from 1 μg of total RNA by Reverse Transcriptase using M-MLV (Promega) and oligo (dT) primers (Promega) according to the manufacturer's protocol. Real-time quantitative PCR (RT-PCR^q) was performed by QuantiTect SYBR Green PCR kit (Qiagen) using ABI PRISM 7900HT Sequence Detection System (Applied Biosystems, USA). Two microliters of template cDNA was added to the final volume of 20 μl of reaction mixture. Real-time PCR cycle parameters included 10 min at 95 °C followed by 40 cycles involving denaturation at 95 °C for 15 s, annealing at 60 °C for 20 s and elongation at 72 °C for 20 s. The sequences of the specific sets of primer for p53, bax, bcl-2, survivin, caspase-3, caspase-9 and β-actin used in this study are given in Table 1. Expressions of selected genes were normalized to β-actin gene, which was used as an internal housekeeping control. All the real-time PCR experiments were performed in triplicate and data expressed as the mean of at least three independent experiments.

2.9. Assays of caspase-3 and caspase-9 enzymes

Activities of caspase-3 and caspase-9 enzymes were measured in A549 cells treated with nickel ferrite nanoparticles at the concentrations of 25, 50 and 100 μg/ml using the standard assay kit (BioVision, Inc.). This assay is based on the principle that activated caspases in apoptotic cells cleave the synthetic substrates to release free chromophore p-nitroanilide (pNA), which is measured at 405 nm. The pNA was generated after specific action of caspase-3 and caspase-9 on tertrapeptide substrates DEVD-pNA and LEHD-pNA, respectively (Berasain et al., 2005; Ahamed et al., 2010b). The reaction mixture consisted of 50 μl of cell extract protein (50 μg), 50 μl of 2× reaction buffer (containing 10 mM dithiothreitol) and 5 μl of 4 mM DEVD-pNA (for caspase-3) or LEHD-pNA (for caspase-9) substrate in a total volume of 105 μl. The reaction mixture was incubated at 37 °C for 1 h and absorbance of the product was measured using microplate reader (Synergy-HT, BioTek) at 405 nm according to manufacturer's instruction. Activities of caspase-3 and caspase-9 enzymes are presented as picomol DEVD-pNA/μg protein and picomol LEHD-pNA/μg protein respectively.

2.10. Protein estimation

Estimation of protein was done using a BCA protein assay kit (Pierce Biotechnology). The BCA protein assay is a detergent-compatible formulation based on bicinchoninic acid (BCA) for the colorimetric detection and quantification of total protein.

2.11. Statistical analysis

All the data represented in this study are means ± SD of three identical experiments made in three replicate. Statistical significance was determined by one-way analysis of variance (ANOVA) followed by Dunnett's multiple comparison test. Significance was ascribed at $p < 0.05$. All analyses were conducted using the Prism software package (GraphPad Software).

3. Results

3.1. Characterization of nickel ferrite nanoparticles

Fig. 1 shows the XRD pattern of nickel ferrite nanopowder that clearly exhibits crystalline nature of this material. The crystallite size has been estimated from the XRD pattern using the Scherrer's equation (Patterson, 1939).

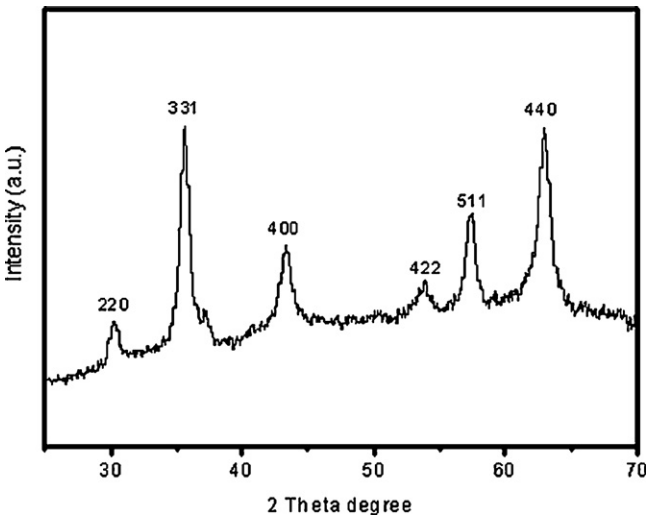

Fig. 1. X-ray diffraction pattern of nickel ferrite nanoparticles.

$$D = \frac{0.9\lambda}{B \cos \theta}$$

where D is the grain size, λ the wavelength of X-ray (1.54056 Å), B the full-width at half-maxima of the diffraction peak (in radian)

The average crystallite size corresponding to the highest peak observed in XRD was found to be 26 ± 17 nm. The presence of sharp structural peaks in XRD patterns and average crystallite size less than 100 nm suggested the nano-crystalline nature of the particles. Fig. 2A and B shows the typical SEM and TEM images of the nickel ferrite nanoparticles respectively. TEM average diameter was calculated from measuring over 100 particles in random fields of TEM view. The average TEM diameter of nickel ferrite nanoparticles was 25 ± 97 nm further supporting the XRD result. The EDX spectrum of nickel ferrite nanoparticles is given in Fig. 2C. The presence of Cu and C signals was from the carbon-coated-copper TEM-grid. The EDX result showing that there is no other elemental impurities present in nickel ferrite nanoparticles used in this study.

The average hydrodynamic size of nickel ferrite nanoparticles suspension in cell culture medium as determined by dynamic light scattering (DLS) was 97 ± 23 nm. The higher size of nanoparticles in aqueous suspension as compared to TEM and XRD sizes might be due to the tendency of particles to aggregate in aqueous state. This finding is supported by other investigators (Bai et al., 2009; Sharma et al., 2009) and has been briefly discussed in our previous publication (Ahamed et al., 2010b).

3.2. Nickel ferrite nanoparticle-induced cytotoxicity

Human lung epithelial A549 cells were exposed to nickel ferrite nanoparticles at the concentrations of 0, 1, 2, 5, 10, 25, 50 and 100 μg/ml for 24 h and cytotoxicity was determined using MTT, NRU and LDH assays. All the three assays have shown that nickel ferrite nanoparticles up to the concentration of 10 μg/ml, did not produce significant cytotoxicity ($p > 0.05$ for each). As the concentration of nanoparticles increased to 25, 50 and 100 μg/ml cytotoxicity was observed in dose-dependent manner. In MTT assay cell viability was significantly decreased to 83%, 76% and 69% for the concentrations of 25, 50 and 100 μg/ml respectively ($p < 0.05$ for each) (Fig. 3A). Fig. 3B shows the results of cell viability obtained by NRU assay. In this assay the cell viability decreased to 84%, 78% and 73% when cells exposed to nickel ferrite nanoparticles at the concentrations of 25, 50 and 100 μg/ml respectively ($p < 0.05$ for each).

Table 1
Sequences of primers used for quantitative real-time PCR.

Target gene	Forward	Reverse
p53	5′-CCCAGCCAAAGAAGAAACCA-3′	5′- TTCCAAGGCCTCATTCAGCT-3′
Survivin	5′-AGAACTGGCCCTTCTTGGAGG-3′	5′-CTTTTTATGTTCCTCTATGGGGTC-3′
bax	5′-TGCTTCAGGGTTTCATCCAG-3′	5′-GGCGGCAATCATCCTCTG-3′
bcl-2	5′-AGGAAGTGAACATTTCGGTGAC-3′	5′-GCTCAGTTCCAGGACCAGGC-3′
Caspase-3	5′-ACATGGCGTGTCATAAAATACC-3′	5′-CACAAAGCGACTGGATGAAC-3′
Caspase-9	5′-CCAGAGATTCGCAAACCAGAGG-3′	5′-GAGCACCGACATCACCAAATCC-3′
β-Actin	5′TCACCCACACTGTGCCCATCTACGA-3′	5′ AGCGGAACCGCTCATTGCCAATGG 3′

A significant LDH leakage in culture media was also observed at 24 h on exposure to 25, 50 and 100 μg/ml concentrations of nickel ferrite nanoparticles ($p < 0.05$ for each) (Fig. 3C). We further determined the correlation between the cell viability (MTT assay) and LDH leakage of treated and untreated cells. A significant negative correlation observed between the cell viability and LDH leakage ($p < 0.05$) (Fig. 4).

3.3. Nickel ferrite nanoparticle-induced oxidative stress

The potential of nickel ferrite nanoparticles to induce oxidative stress was assessed by measuring the ROS and GSH levels in human lung epithelial A549 cells. Fig. 5A shows that the nickel ferrite nanoparticles significantly induced the intracellular production of ROS ($p < 0.05$). We further noted that co-exposure of L-ascorbic acid (an antioxidant) effectively prevented the ROS generation induced by nickel ferrite nanoparticles. ROS level was reduced up to control level for nickel ferrite nanoparticles in the presence of ascorbic acid (Fig. 5A, $p < 0.05$). When the nickel ferrite nanoparticles induced ROS was 1.52-fold, in the presence of ascorbic acid it was reduced and found to be 1.06-fold of control level.

Fig. 5B shows that nickel ferrite nanoparticles significantly reduced the intracellular level of GSH ($p < 0.05$). Further, co-exposure of an antioxidant (L-ascorbic acid) significantly prevented the reduction of GSH due to nickel ferrite nanoparticles (Fig. 5B, $p < 0.05$). GSH reduction due to nickel ferrite nanoparticles exposure was 1.43-fold as compared to untreated control cells, where as in the presence of ascorbic acid there was no significant reduction in GSH as compared to control (1.07-fold). These results clearly demonstrated that nickel ferrite nanoparticles induced oxidative stress in A549 cells by induction of oxidants (ROS) and depletion of antioxidant (GSH).

3.4. Nickel ferrite nanoparticle-induced apoptosis

It has widely been reported that ROS generation and oxidative stress leads to DNA damage and ultimately apoptotic cell death (Paz-Elizur et al., 2008; Ahamed et al., 2010b,c). In this study, quan-

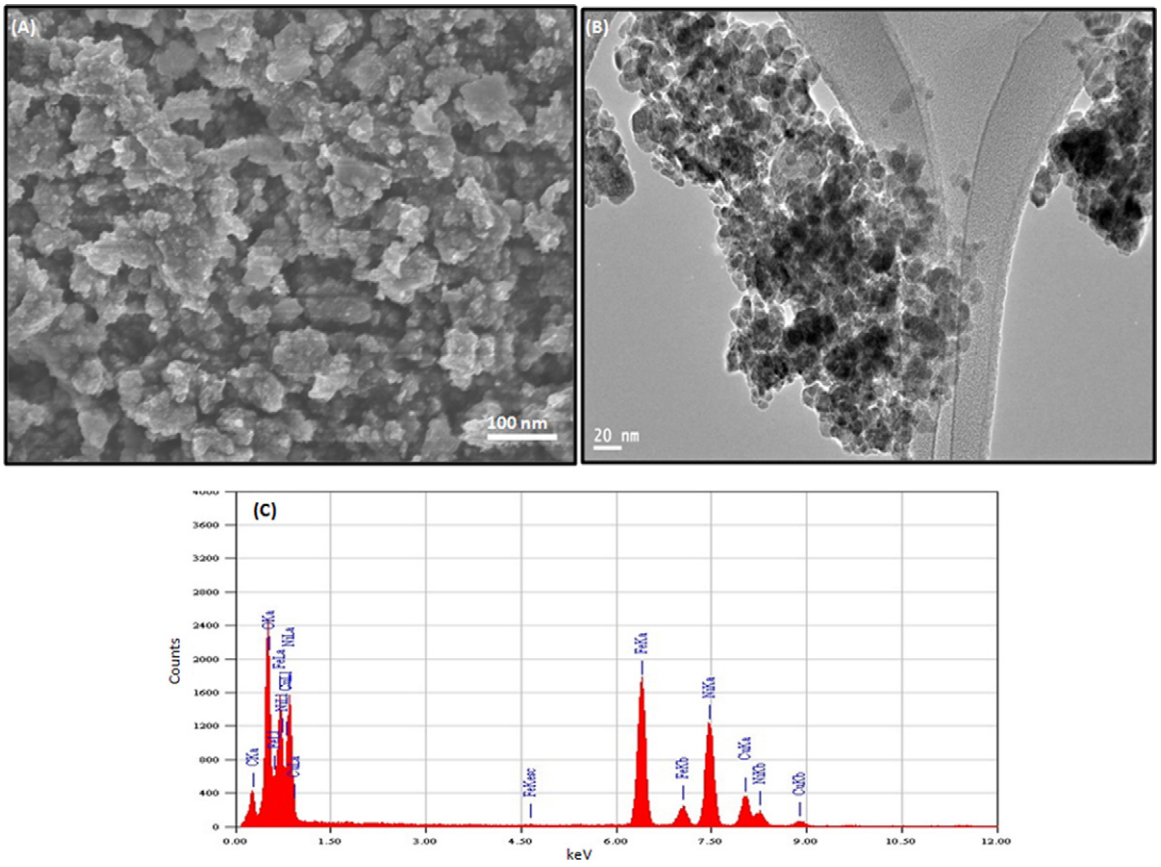

Fig. 2. Electron microscopy characterization of nickel ferrite nanoparticles. (A) Field emission scanning electron microscope image, (B) field emission transmission electron microscope image, and (C) energy dispersive X-ray spectrum.

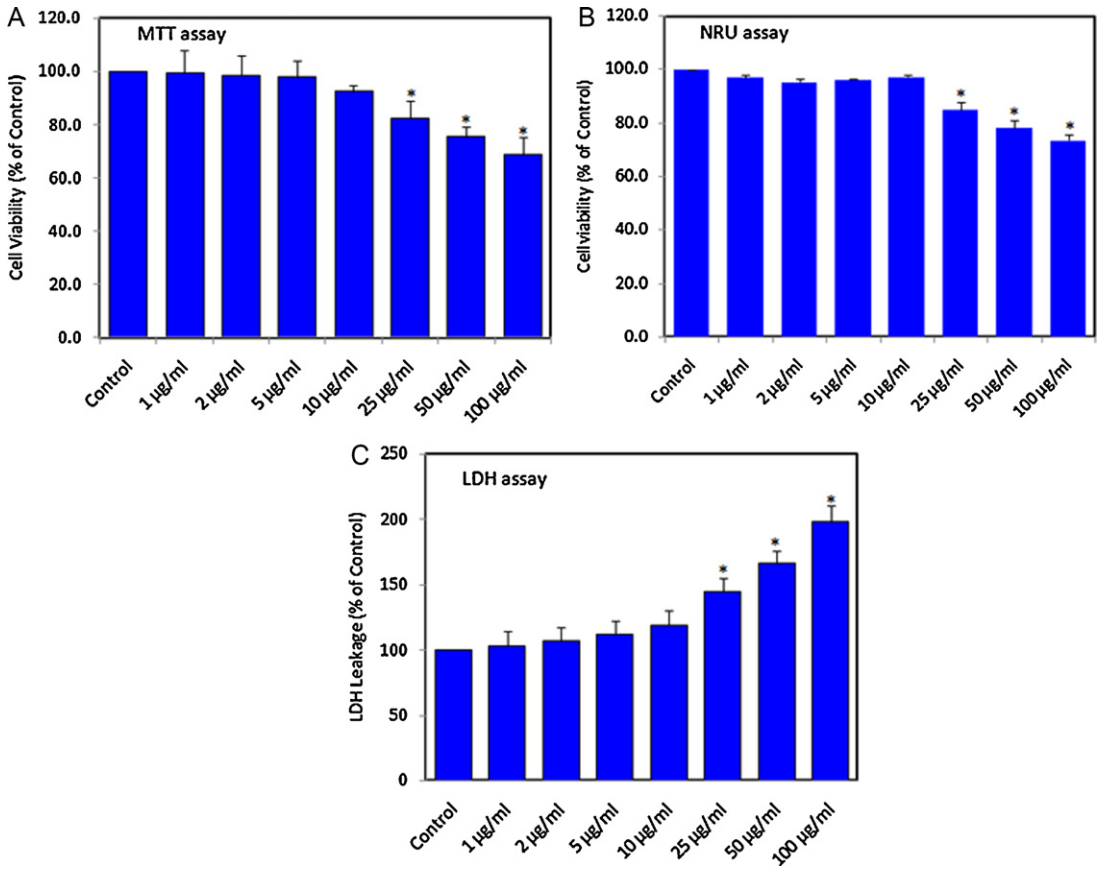

Fig. 3. Nickel ferrite nanoparticle-induced cytotoxicity in A549 cells. Cells were treated with nickel ferrite nanoparticles at the concentrations of 0, 1, 2, 5, 10, 25, 50 and 100 μg/ml for 24 h. At the end of treatment cytotoxicity parameters were determined as described in Section 2. (A) MTT assay (B) NRU assay and (C) LDH leakage assay. Data represented are mean ± SD of three identical experiments made in three replicate. *Statistically significant difference as compared to the controls ($p < 0.05$ for each).

titative real-time PCR was utilized to analyze the mRNA levels of apoptotic markers (e.g. p53, survivin, bax, bcl-2, caspase-3 and caspase-9) in A549 cells exposed nickel ferrite nanoparticles at a concentration of 100 μg/ml for 24 h. Results showed that the mRNA levels of these apoptotic markers were significantly altered in A549 cells due to nickel ferrite nanoparticles exposure (Fig. 6, $p < 0.05$ for each). The mRNA level of tumor suppression gene p53 was 1.66-fold higher (Fig. 6A, $p < 0.05$) while the m RNA level of survivin, a well-known member of the inhibitor of the apoptosis protein (IAP) family was 1.34-fold lower (Fig. 6B, $p < 0.05$) in treated cells as compared to the control. We further found higher mRNA expression of pro-apoptotic gene bax (1.43-fold) (Fig. 6C, $p < 0.05$) and lower expression of anti-apoptotic gene bcl-2 (1.41 fold) (Fig. 6D, $p < 0.05$) in exposed cells than those of untreated cells. Moreover, we examined the effect of nickel ferrite nanoparticles on the mRNA expression of caspase-3 and caspase-9 enzymes. The expression of caspase-3 was 1.38-fold (Fig. 6E, $p < 0.05$) and caspase-9 (Fig. 6F, $p < 0.05$) was 1.31-fold higher in treated cells in comparison with untreated control cells. To support our hypothesis of apoptosis induction by nickel ferrite nanoparticles, we further examined the activities of caspas-3 and caspase-9 enzymes at the concentrations of 25, 50 and 100 μg/ml. Results showed that nickel ferrite nanoparticles induced the activities of both apoptotic enzymes in a dose-dependent manner (Fig. 7A and B).

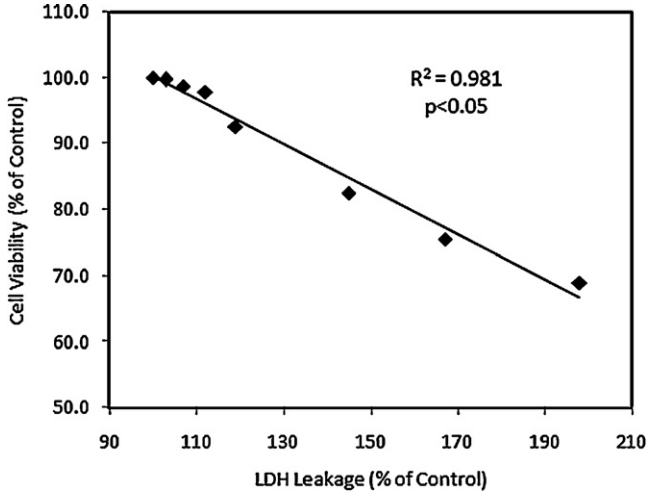

Fig. 4. Significant negative correlation between the cell viability and LDH leakage after 24 h exposure to 0, 1, 2, 5, 10, 25, 50 and 100 μg/ml of nickel ferrite nanoparticles.

4. Discussion

Due to wide spread application of magnetic nanoparticles it is imperative to evaluate their potential risks to the environment and human health. Results published in the scientific literature concerning toxic potential of iron-based nanoparticles are conflicting. These nanoparticles have been shown to generate toxicity (Zhu et al., 2010; Apopa et al., 2009; Lunov et al., 2010; Park et al., 2010), while others report that they do not only show good biocompatibility but also exert very low toxicity (Mahmoudi et al., 2009, 2010; Song et al., 2010). One of our previous studies has shown the cytotoxicity and oxidative caused by nickel (Ni) nanoparticles in human lung epithelial cells (Ahamed, 2011). This prompted us

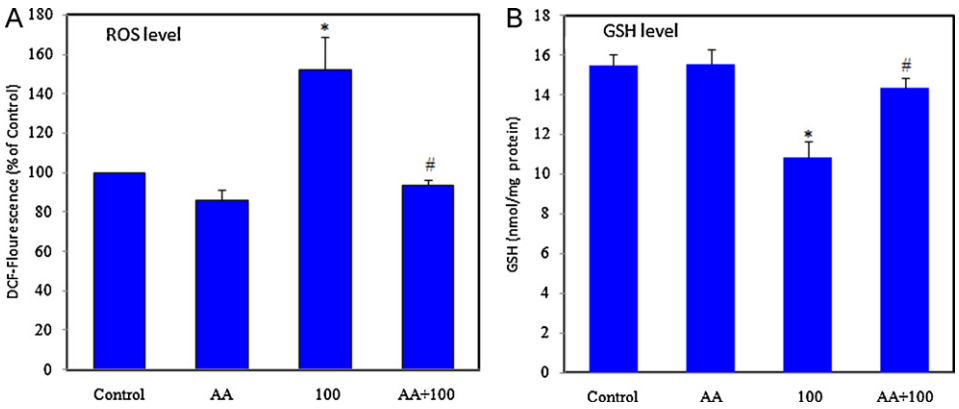

Fig. 5. Nickel ferrite nanoparticle-induced oxidative stress in A549 cells. Cells were treated with nickel ferrite nanoparticles at a concentration of 100 μg/ml for 24 h. L-Ascorbic acid (AA) was co-exposed with or without nickel ferrite nanoparticles. At the end of treatment ROS and GSH levels were determined as described in Section 2. AA and 100 refers to concentrations of ascorbic acid (1.5 mM) and nickel ferrite nanoparticles (μg/ml) respectively. (A) ROS level and (B) GSH level. Data represented are mean ± SD of three identical experiments made in three replicate. *Statistically significant difference in ROS generation and GSH depletion as compared to the controls ($p < 0.05$ for each). #Significant inhibitory effect of L-ascorbic acid (AA) on ROS generation and GSH depletion ($p < 0.05$ for each).

to investigate the toxicity of nickel ferrite nanoparticle ($NiFe_2O_4$), which has both Ni and Fe_2O_4 components and has tremendous potential for biological applications. Therefore in this study, toxic responses of nickel ferrite nanoparticles to human lung epithelial A549 cells were investigated. Our results demonstrated that exposure of nickel ferrite nanoparticles to A549 cells cause cytotoxicity and oxidative stress. We have also observed apoptotic response of nickel ferrite nanoparticles in A549 cells for which ROS generation and oxidative stress may be attributed as one of the possible cause.

We used more than one assay to evaluate the cytotoxicity of nickel ferrite nanoparticles to get more reliable data. The cytotoxicity assays employed were mitochondrial function (MTT), neutral red uptake (NRU) and membrane integrity (LDH leakage). In general, all the three assays are frequently used to assess the cytotoxicity of nanoparticles in different kinds of cell lines (Sharma et al., 2009; Ahamed et al., 2010c; Akhtar et al., 2010a; Mahmoudi et al., 2009; Barillet et al., 2010). All the three assays revealed that the nickel ferrite nanoparticles exert significant cytotoxicity to A549 cells in dose-dependent manner in the concentration range of 25–100 μg/ml. Nickel ferrite nanoparticles at the concentration of ≤10 μg/ml did not produce significant cytotoxicity to A549 cells. Our cytotoxicity data is in accordance to the recent results of Tomitaka et al. (2009). They investigated the cytotoxic response of nickel ferrite nanoparticles (20–30 nm) to HeLa cells for the concentrations of 10 and 100 μg/ml. Results showed that nickel ferrite nanoparticles at low concentration (10 μg/ml) did not produce

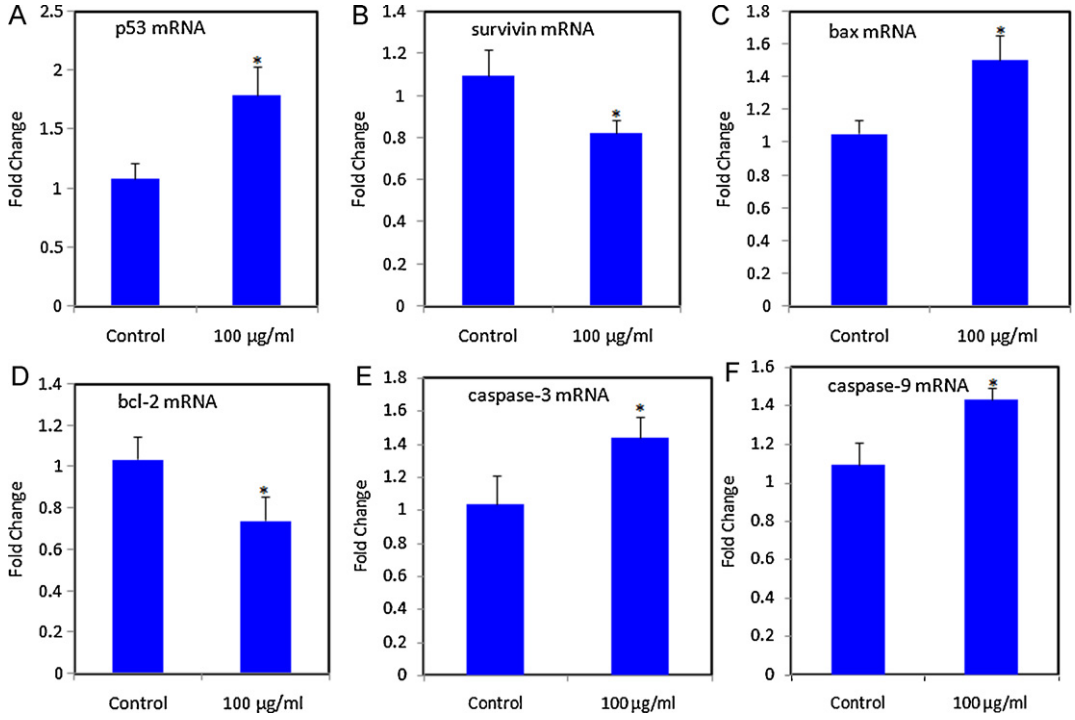

Fig. 6. Effect of nickel ferrite nanoparticle on mRNA expression level of apoptotic markers in A549 cells. Cells were treated with nickel ferrite nanoparticles at a concentration of 100 μg/ml for 24 h. Quantitative real-time PCR (RT-PCR^q) was performed by QuantiTect SYBR Green PCR kit using ABI PRISM 7900HT Sequence Detection System. The β-actin was used as the internal control to normalize the data. Nickel ferrite nanoparticle-induced alterations in mRNA expression levels are expressed in relative quantity compared with those for the respective unexposed control cells. Data represented are mean ± SD of three identical experiments made in three replicate. *Statistically significant difference as compared to the controls ($p < 0.05$ for each).

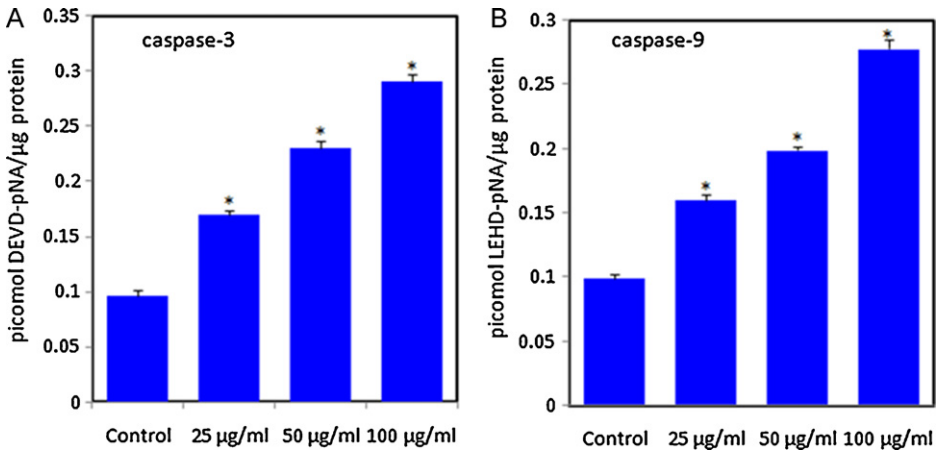

Fig. 7. Nickel ferrite nanoparticles increased the activities of Caspase-3 and Caspase-9 enzymes in A549 cells. Cells were treated with nickel ferrite nanoparticles at the concentrations of 0, 25, 50 and 100 μg/ml for 24 h. At the end of treatment activities of caspase-3 and caspase-9 enzymes were determined using BioVision assay kit as described in Section 2. (A) Caspase-3 activity and (B) caspase-9 activity. Data represented are mean ± SD of three identical experiments made in three replicate. *Statistically significant difference as compared to the controls ($p < 0.05$ for each).

cytotoxicity while the higher concentration (100 μg/ml) significantly reduced the viability of HeLa cells. As with most published work in nanotoxicology, the high concentration-induced cytotoxicity observed in this study may be difficult to translate to a realistic human exposure scenario. We believe these data are positioned to provide a springboard for other researchers to create mechanistic pathways involved in nickel ferrite nanoparticles induced apoptosis and provide knowledge for this important deficiency in this rapidly evolving area of human exposure concern.

Oxidative stress has been proposed as a common mechanism of cell damage induced by many types of nanoparticles (Park et al., 2008, 2010; Ahamed et al., 2010a; Stone and Donaldson, 2006). For example, iron-based nanoparticles produced toxicity to biological systems by generating ROS (Stroh et al., 2004; Zhu et al., 2010; Apopa et al., 2009). In our previous study, we found that Ni nanoparticles induced cytotoxicity in A549 cells through ROS generation and lipid peroxidation (Ahamed, 2011). In the present study, we hypothesized that the nickel ferrite nanoparticles induced toxic response in A549 cells through ROS generation and GHS depletion. The cell has a number of mechanisms of protection against oxidative damage including direct interaction with anti-oxidants. Indeed, co-treatment with the antioxidant L-ascorbic acid mitigated the ROS generation and GSH depletion in A549 cells due to nickel ferrite nanoparticles exposure, suggesting that oxidative stress may be responsible for the toxicity of these nanoparticles.

ROS has been suggested to be signaling molecule for the initiation and execution of the apoptotic death program (Ott et al., 2007; Rana, 2008). The production of ROS, in particular, has also been associated with programmed cell death in many conditions such as stroke, inflammation, ischemia, lung edema and neuro-degeneration (Kannan and Jain, 2000; Bai and Meng, 2005). We analyzed the mRNA expression of six genes; p53, survivin, bax, bcl-2, caspase-3 and caspase-9 in response to nickel ferrite nanoparticles exposure in A549 cells, because apoptosis is controlled through these pathways. Quantitative real-time PCR results showed that nickel ferrite nanoparticles up-regulated mRNA level of cell cycle checkpoint protein p53 and pro-apoptotic protein bax. Expression of anti-apoptotic proteins survivin and bcl-2 was down-regulated in cells exposed to nickel ferrite nanoparticles. Furthermore, both the mRNA expressions and activities of apoptotic enzymes caspase-3 and caspase-9 enzymes were higher in nanoparticles treated cells. Taken together, up-regulation of p53 and down-regulation of survivin leads to activation of pro-apoptotic members of bcl-2 family, such as bax induces permeabilization of the outer mitochondrial membrane, which releases soluble proteins from the intermembrane space into the cytosol, where they promote caspase activation (Fuentes-Prior and Salvesen, 2004; Youle and Strasser, 2008). The best studied of these proteins is cytochrome *c*, which binds to apoptosis protease activating factor-1 (Apaf-1) and leads to the assembly of an apoptosome complex. This apoptosome can bind procaspase-9 and cause its auto-activation through a conformational change. Once initiated caspase-9 goes on to activate caspase-3 (effector caspase), which cleaves substrates at aspartate residues and activation of this proteolytic activity appears to be an event in apoptosis (Timmer and Salvesen, 2007). Survivin inhibition also induce the activation of caspase-3 (Blanc-Brude et al., 2002) and caspase-9 enzymes (Marusawa et al., 2003). These quantitative real-time PCR results are supported by our previous studies where Western blot results demonstrated that ZnO and CuO nanoparticles significantly up-regulated the expression p53 and bax, and down-regulated survivin and bcl-2 in A549 cells (Ahamed et al., 2010c, 2011).

In conclusion, we have shown that nickel ferrite nanoparticles produce significant cytotoxicity to A549 cells in dose-dependent manner in the concentration range of 25–100 μg/ml. This nanocrystalline particle was also found to induce oxidative stress by induction of ROS level and depletion GSH level, while co-treatment with the antioxidant L-ascorbic acid mitigated the ROS generation and GSH depletion. Furthermore, quantitative real-time PCR analysis displayed that mRNA levels of proteins involved in the apoptosis were altered by nickel ferrite nanoparticles. Overall, our data suggesting that nickel ferrite nanoparticles may induce apoptosis in A549 cells through ROS generation via p53, survivin, bax/bcl-2 and caspase pathways. This *in vitro* study showed the induction of apoptosis by nickel ferrite nanoparticles warrants further investigation to determine if *in vivo* exposure consequences may exist for nickel ferrite nanoparticles application.

Conflict of interest statement

The authors declare that there are no conflicts of interest.

Acknowledgment

Financial assistance from King Abdullah Institute for Nanotechnology (KAIN) is thankfully acknowledged.

References

Ahamed, M., Karns, M., Goodson, M., Rowe, J., Hussain, S., Schlager, J., Hong, Y., 2008. DNA damage response to different surface chemistry of silver nanoparticles in mammalian cells. Toxicol. Appl. Pharmacol. 233, 404–410.

Ahamed, M., AlSalhi, M.S., Siddiqui, M.K.J., 2010a. Silver nanoparticle applications and human health. Clin. Chim. Acta 411, 1841–1848.

Ahamed, M., Posgai, R., Gorey, T.J., Nielsen, M., Hussain, S., Rowe, J., 2010b. Silver nanoparticles induced heat shock protein 70, oxidative stress and apoptosis in *Drosophila melanogaster*. Toxicol. Appl. Pharmacol. 242, 263–269.

Ahamed, M., Siddiqui, M.A., Akhtar, M.J., Ahmad, I., Pant, A.B., Alhadlaq, H.A., 2010c. Genotoxic potential of copper oxide nanoparticles in human lung epithelial cells. Biochem. Biophys. Res. Commun. 396, 578–583.

Ahamed M., 2011. Toxic response of nickel nanoparticles in human lung epithelial A549 cells. Toxicol. In Vitro. doi:10.1016/j.tiv.2011.02.015.

Ahamed, M., Akhtar, M.J., Raja, M., Ahmad, I., Siddiqui, M.K.J., AlSalhi, M.S., Alrokayan, S.A., 2011. ZnO nanorod induced apoptosis via p53, survivin and bax/bcl-2 pathways mediated by oxidative stress in human alveolar adenocarcinoma cells. Nanomedicine Accepted.

Akhtar, M.J., Ahamed, M., Kumar, S., Siddiqui, S., Patil, G., Ashquin, M., Ahmad, I., 2010a. Nanotoxicity of pure silica mediated through oxidant generation rather than glutathione depletion in human lung epithelial cells. Toxicology 276, 95–102.

Akhtar, M.J., Kumar, S., Murthy, R.C., Ashquin, M., Khan, M.I., Patil, G., Ahmad, I., 2010b. The primary role of iron-mediated lipid peroxidation in the differential cytotoxicity caused by two varieties of talc nanoparticles on A549 cells and lipid peroxidation inhibitory effect exerted by ascorbic acid. Toxicol. In Vitro 24, 1139–1147.

Apopa, P.L., Qian, Y., Shao, R., Guo, N.L., Schwegler-Berry, D., Pacurari, M., et al., 2009. Iron oxide nanoparticles induce human microvascular endothelial cell permeability through reactive oxygen species production and microtubule remodeling. Part. Fibre Toxicol. 6, 1.

Asharani, P.V., Mun, G.K., Hande, M.P., Valiyaveettil, S., 2009. Cytotoxicity and genotoxicity of silver nanoparticles in human cells. ACS Nano. 3, 279–290.

Bai, J., Meng, Z., 2005. Effects of sulfur dioxide on apoptosis-related gene expressions in lungs from rats. Regul. Toxicol. Pharmacol. 43, 272–279.

Bai, W., Zhang, Z., Tian, W., He, X., Ma, Y., Zhao, Y., Chai, Z., 2009. Toxicity of zinc oxide nanoparticles to zebrafish embryo: a physicochemical study of toxicity mechanism. J. Nanopart. Res. 12, 1645–1654.

Baldi, G., Bonacchi, D., Franchini, M.C., Gentili, D., Lorenzi, G., Ricci, A., et al., 2007. Synthesis and coating of cobalt ferrite nanoparticles: a first step toward the obtainment of new magnetic nanocarriers. Langmuir 23, 4026–4028.

Barillet, S., Jugan, M.L., Laye, M., Leconte, Y., Herlin-Boime, N., Reynaud, C., Carrière, M., 2010. *In vitro* evaluation of SiC nanoparticles impact on A549 pulmonary cells: cyto-, genotoxicity and oxidative stress. Toxicol. Lett. 198, 324–330.

Beji, Z., Hanini, A., Smiri, L.S., Gavard, J., Kacem, K., Villain, F., et al., 2010. Magnetic properties of Zn-substituted $MnFe_2O_4$ nanoparticles synthesized in polyol as potential heating agents for hyperthermia. Evaluation of their toxicity on endothelial cells. Chem. Mater. 22, 5420–5429.

Berasain, C., García-Trevijano, E.R., Castillo, J., Erroba, E., Santamaria, M., Lee, D.C., 2005. Novel role for amphiregulin in protection from liver injury. J. Biol. Chem. 280, 19012–19020.

Blanc-Brude, O.P., Yu, J., Simosa, H., Conte, M.S., Sessa, W.C., Altieri, D.C., 2002. Inhibitor of apoptosis protein survivin regulates vascular injury. Nature Med. 8, 987–994.

Borenfreund, E., Puerner, J.A., 1984. A simple quantitative procedure using monolayer cultures for cytotoxicity assays. J. Tissue Culture Method 9, 7–9.

Chertok, B., Moffat, B.A., David, A.E., Yu, F., Bergemann, C., Ross, B.D., Yang, V.C., 2008. Iron oxide nanoparticles as a drug delivery vehicle for MRI monitored magnetic targeting of brain tumors. Biomaterials 29, 487–496.

Chougule, M., Patel, A.R., Sachdeva, P., Jackson, T., Singh, M., 2010. Anticancer activity of Noscapine, an opioid alkaloid in combination with cisplatin in human non-small cell lung cancer. Lung Cancer, doi:10.1016/j.lungcan.2010.06.002.

Ellman, G.I., 1959. Tissue sulfhydryl groups. Arch. Biochem. Biophys. 82, 70–77.

Farnebo, M., Bykov, V.N., Wiman, K.G., 2010. The p53 tumor suppressor: a master regulator of diverse cellular processes and therapeutic target in cancer. Biochem. Biophys. Res. Commun. 396, 85–89.

Fuentes-Prior, P., Salvesen, G.S., 2004. The protein structures that shape caspase activity, specificity, activation and inhibition. J. Biochem. 384, 201–232.

Gao, C., Wang, A.Y., 2009. Significance of increased apoptosis and bax expression in human small intestinal adenocarcinoma. J. Histochem. Cytochem. 57, 1139–1148.

Kannan, K., Jain, S.K., 2000. Oxidative stress and apoptosis. Pathophysiology 7, 153–163.

Lee, J.H., Huh, Y.M., Jun, Y.W., Seo, J.W., Jang, J.T., Song, H.T., et al., 2007. Artificially engineered magnetic nanoparticles for ultra-sensitive molecular imaging. Nat. Med. 13, 95–99.

Lunov, O., Syrovets, T., Büchele, B., Jiang, X., Röcker, C., Tron, K., et al., 2010. The effect of carboxydextran-coated superparamagnetic iron oxide nanoparticles on c-Jun N-terminal kinase-mediated apoptosis in human macrophages. Biomaterials 31, 5063–5071.

Mahmoudi, M., Sant, S., Wang, B., Laurent, S., Sen, T., 2010. Superparamagnetic iron oxide nanoparticles (SPIONs): development, surface modification and applications in chemotherapy. Adv. Drug Deliv. Rev., doi:10.1016/j.addr.2010.05.006.

Mahmoudi, M., Simchi, A., Milani, A.S., Stroeve, P., 2009. Cell toxicity of superparamagnetic iron oxide nanoparticles. J. Colloid Interf. Sci. 336, 510–518.

Marusawa, H., Matsuzawa, S., Welsh, K., Zou, H., Armstrong, R., Tamm, I., Reed, J.C., 2003. HBXIP functions as a cofactor of survivin in apoptosis suppression. EMBO J. 22, 2729–2740.

Mossman, T., 1983. Rapid colorimetric assay for cellular growth and survival: application to proliferation and cytotoxicity assays. J. Immunol. Methods 65, 55–63.

Nel, A., Xia, T., Madler, L., Li, N., 2006. Toxic potential of materials at the nanolevel. Nature 311, 622–627.

Ott, M., Gogvadze, V., Orrenius, S., Zhivotovsky, B., 2007. Mitochondria, oxidative stress and cell death. Apoptosis 12, 913–922.

Park, E.J., Kimb, H., Kimb, Y., Yic, J., Choid, K., Park, K., 2010. Inflammatory responses may be induced by a single intratracheal instillation of iron nanoparticles in mice. Toxicology 275, 65–71.

Park, E.J., Yi, J., Chung, K.H., Ryu, D.Y., Choi, J., Park, K., 2008. Oxidative stress and apoptosis induced by titanium dioxide nanoparticles in cultured BEAS-2B cells. Toxicol. Lett. 180, 222–229.

Patterson, A.L., 1939. The Scherrer formula for X-ray particle size determination. Phys. Rev. 56, 978–982.

Paz-Elizur, T., Sevilya, Z., Leitner-Dagan, Y., Elinger, Y., Roisman, L.C., Livneh, Z., 2008. DNA repair of oxidative DNA damage in human carcinogenesis: potential application for cancer risk assessment and prevention. Cancer Lett. 266, 60–72.

Rana, S., Gallo, A., Srivastava, R.S., Misra, R.K., 2007. On the suitability of nanocrystalline ferrites as a magnetic carrier for drug delivery: functionalization, conjugation and drug release kinetics. Acta Biomater. 3, 233–242.

Rana, S.V., 2008. Metals and apoptosis: recent developments. J. Trace Elem. Med. Biol. 22, 262–284.

Ryan, B.M., O'Donovan, N., Duffy, M.J., 2009. Survivin: a new target for anti-cancer therapy. Canc. Treat. Rev. 35, 553–562.

Sánchez-Pérez, Y., Chirino, Y.I., Osornio-Vargas, A.R., Morales-Bárcenas, R., Gutiérrez-Ruíz, C., Vázquez-López, I., García-Cuellar, C.M., 2009. DNA damage response of A549 cells treated with particulate matter (PM_{10}) of urban air pollutants. Cancer Lett. 278, 192–200.

Sharma, V., Shukla, R.K., Saxena, N., Parmar, D., Das, M., Dhawan, A., 2009. DNA damaging potential of zinc oxide nanoparticles in human epidermal cells. Toxicol. Lett. 185, 211–218.

Sherr, C.J., 2004. Principles of tumor suppression. Cell 11, 235–246.

Siddiqui, M.A., Kashyap, M.P., Kumar, V., Al-Khedhairy, A.A., Musarrat, J., Pant, A.B., 2010. Protective potential of trans-resveratrol against 4-hydroxynonenal induced damage in PC12 cells. Toxicol. In Vitro 24, 1592–1598.

Song, M.M., Song, W.J., Bi, H., Wang, J., Wu, W.L., Sun, J., Yu, M., 2010. Cytotoxicity and cellular uptake of iron nanowires. Biomaterials 31, 1509–1519.

Stone, V., Donaldson, K., 2006. Nanotoxicology: signs of stress. Nat. Nanotech. 1, 23–24.

Stroh, A., Zimmer, C., Gutzeit, C., Jakstadt, M., Marschinke, F., Jung, T., et al., 2004. Iron oxide particles for molecular magnetic resonance imaging cause transient oxidative stress in rat macrophages. Free Radic. Biol. Med. 36, 976–984.

Sun, C., Lee, J.H., Zhang, M., 2008. Magnetic nanoparticles in MR imaging and drug delivery. Adv. Drug Deliv. Rev. 60, 1252–1265.

Takadera, T., Ohyashiki, T., 2007. Caspase-dependent apoptosis induced by calcineurin inhibitors was prevented by glycogen synthase kinase-3 inhibitors in cultured rat cortical cells. Brain Res. 1133, 20–26.

Tang, X., Guo, Y., Nakamura, K., Huang, H., Hamblin, M., Chang, L., Villacorta, L., Yin, K., Ouyang, H., Zhang, J., 2010. Nitroalkenes induce rat aortic smooth muscle cell apoptosis via activation of caspase-dependent pathways. Biochem. Biophys. Res. Commun. 397, 239–244.

Timmer, J.C., Salvesen, G.S., 2007. Caspase substrates. Cell Death Differ. 14, 66–72.

Tomitaka, A., Hirukawa, A., Yamada, T., Morishita, S., Takemura, Y., 2009. Biocompatibility of various ferrite nanoparticles evaluated by *in vitro* cytotoxicity assays using HeLa cells. J. Magnetism Magnet. Mater. 321, 1482–1484.

Tomitaka, A., Koshi, T., Hatsugai, S., Yamada, T., Takemura, Y., 2010. Magnetic characterization of surface-coated magnetic nanoparticles for biomedical application. J. Maget. Magnetism. Mater., doi:10.1016/j.jmmm.2010.11.054.

Wang, H., Joseph, J.A., 1999. Quantifying cellular oxidative stress by dichlorofluorescin assay using microplate reader. Free Radic. Biol. Med. 27, 612–616.

Willard, M.A., Kurihara, L.K., Carpenter, E.E., Calvin, S., Harris, V.G., 2004. Chemically prepared magnetic nanoparticles. Int. Mat. Rev. 49, 125–170.

Wroblewski, F., LaDue, J.S., 1955. Lactate dehydrogenase activity in blood. Proc. Soc. Exp. Biol. Med. 90, 210–213.

Ye, S.-F., Wu, Y.-H., Hou, Z.-Q., Zhang, Q.-Q., 2009. ROS and NF-κB are involved in upregulation of IL-8 in A549 cells exposed to multi-walled carbon nanotubes. Biochem. Biophys. Res. Commun. 379, 643–648.

Yin, H., Too, H.P., Chow, G.M., 2005. The effects of particle size and surface coating on the cytotoxicity of nickel ferrite. Biomaterials 26, 5818–5858.

Youle, R.J., Strasser, A., 2008. The BCL-2 protein family: opposing activities that mediate cell death. Nat. Rev. Mol. Cell Biol. 9, 47–59.

Zhang, J., Zhang, T., Ti, X., Shi, J., Wu, C., Ren, X., Yin, X., 2010. Curcumin promotes apoptosis in A549/DDP multidrug-resistant human lung adenocarcinoma cells through an miRNA signaling pathway. Biochem. Biophys. Res. Commun., 1–6, 2010.

Zhu, M.T., Wang, Y., Feng, W.Y., Wang, B., Wang, M., Ouyang, H., Chai, Z.F., 2010. Oxidative stress and apoptosis induced by iron oxide nanoparticles in cultured human umbilical endothelial cells. J. Nanosci. Nanotechnol. 10, 8584–8590.